Journal of Applied Physics

RESEARCH ARTICLE | APRIL 22 2025

Angle-asymmetric thermal radiation via efficient inverse design of multi-layer magneto-optical films

Zihe Chen ; Cheng Yuan ; Zhiqiang Wang ; Wubin Kong; Run Hu

Check for updates

J. Appl. Phys. 137, 163102 (2025)
https://doi.org/10.1063/5.0266903

View Online
Export Citation

Articles You May Be Interested In

Ultra-efficient machine learning design of nonreciprocal thermal absorber for arbitrary directional and spectral radiation

J. Appl. Phys. (November 2023)

Study of the Relationship between the VIS-NIR Continuum of Scattered Zenith Solar Radiation and the Atmospheric Meteorological Conditions

AIP Conf. Proc. (April 2007)

Multi-channel nonreciprocal radiation of transverse electric wave with photonic crystal heterostructure

Appl. Phys. Lett. (November 2024)

24 April 2025 09:27:29

Nanotechnology & Materials Science
Optics & Photonics
Impedance Analysis
Scanning Probe Microscopy
Sensors
Failure Analysis & Semiconductors

Unlock the Full Spectrum.
From DC to 8.5 GHz.
Your Application. Measured.
Find out more
Zurich Instruments

AIP Publishing

Journal of Applied Physics ARTICLE pubs.aip.org/aip/jap

Angle-asymmetric thermal radiation via efficient inverse design of multi-layer magneto-optical films

Cite as: J. Appl. Phys. **137**, 163102 (2025); doi: 10.1063/5.0266903
Submitted: 21 February 2025 · Accepted: 1 April 2025 ·
Published Online: 22 April 2025

View Online Export Citation CrossMark

Zihe Chen,[1] Cheng Yuan,[2] Zhiqiang Wang,[3] Wubin Kong,[3] and Run Hu[1,4,a)]

AFFILIATIONS

[1]School of Energy and Power Engineering, Huazhong University of Science and Technology, Wuhan 430074, China
[2]Wuhan Fiberhome Fuhua Electric Co., Ltd., Wuhan 430074, China
[3]School of Electrical and Electronic Engineering, Huazhong University of Science and Technology, Wuhan 430074, China
[4]Department of Applied Physics, Kyung Hee University, Yongin-si, Gyeonggi-do 17104, Republic of Korea

[a)]**Author to whom correspondence should be addressed:** hurun@hust.edu.cn

ABSTRACT

The broad-band, non-directional, and reciprocal properties of traditional thermal radiation significantly limit the precise control and efficient utilization of thermal radiation energy. In recent years, nonreciprocal thermal radiation (NTR) has been proposed with a magneto-optical effect or spatiotemporal modulation; however, most existing NTRs are only achieved with a specific zenith angle (θ) without considering the azimuthal angles (φ), which actually is a nominal NTR and not enough for practical angularly asymmetric thermal radiation (ATR) control. Therefore, we employ the Monte Carlo tree algorithm to optimize the multi-layer structure with magneto-optical materials, which can realize ATR with narrow azimuth (φ: 165°–195°) at a given zenith angle ($\theta = 30°$) and wavelength ($\lambda = 16\,\mu$m). The underlying mechanism is primarily attributed to the excitation of the magneto-optical effect and cavity resonance, which is corroborated by the analysis of a magnetic field distribution. Furthermore, we investigate the impact of the layer number and the zenith angle on the ATR. The proposed design algorithm is, in general, that can be extended to any given zenith angle and azimuthal angle and also paves the way for novel applications in areas, such as directional radiative cooling and thermal focusing.

24 April 2025 09:27:29

© 2025 Author(s). All article content, except where otherwise noted, is licensed under a Creative Commons Attribution-NonCommercial-NoDerivs 4.0 International (CC BY-NC-ND) license (https://creativecommons.org/licenses/by-nc-nd/4.0/). https://doi.org/10.1063/5.0266903

I. INTRODUCTION

Thermal radiation, as a fundamental way of heat transfer,[1–3] has been widely applied, including energy conversion,[4–7] imaging,[8–10] and sensing.[11–13] Actually, any objects above zero-Kelvin temperature will emit thermal radiation energy externally via electromagnetic waves ranging from near-ultraviolet to long-infrared wavelength. Conventionally, thermal radiation is characterized as an incoherent source with broadband and nondirectional emission properties. Nevertheless, thermal radiation at undesirable wavelengths and directions frequently leads to a reduction in efficiency and performance.[14,15] To address these challenges, various strategies have been explored to control the wavelength and angular responses of thermal radiation, such as surface plasmon gratings,[16] metasurfaces,[17,18] and photonic crystals,[19,20] but most of them only modulate the wavelength of thermal radiation. The inherent reciprocal limitations imposed by Lorentz reciprocity result in that thermal radiation is typically emitted symmetrically relative to the normal direction.[15] Symmetric thermal radiation originates from the symmetric band dispersion inherent in reciprocal photon systems, where $\omega(k) = \omega(-k)$.[21] At first glance, any manifestation of asymmetric angular thermal radiation seems to contradict the principles of reciprocity. However, recent theoretical breakthroughs have revealed that asymmetric radiation modes can indeed be realized within reciprocal systems by integrating metasurfaces with carefully engineered non-local modes. Examples include bound states in the continuum within phase gradient metasurfaces[22] and the coupling of grating modes to surface phonon polaritons in silicon carbide (SiC).[23] Additionally, the design of asymmetric sawtooth structures has been shown to produce angularly asymmetric thermal radiation,[24,25] though the fabrication of such aperiodic structures introduces considerable complexity.

Alternatively, nonreciprocal materials, such as magneto-optical materials and Weyl semimetals, offer a promising pathway to break

© Author(s) 2025

the symmetric band dispersion in photonic systems, achieving $\omega(k) \neq \omega(-k)$ through the interaction between photons and magnetic fields.[26] Both theoretical and experimental studies have demonstrated that by combining magneto-optical effects with mechanisms, such as guided mode resonance,[26–30] epsilon-near-zero (ENZ) modes,[31–33] Tamm states,[34–36] and other plasmonic resonances, ATR can be achieved across both narrow and broad spectral bands. These advancements open new possibilities for controlling thermal radiation in ways that were previously unattainable. However, these efforts have predominantly focused on zenith angle (θ) -dependent asymmetric thermal radiation, without considering its behavior across azimuthal angles (φ). Shi *et al.* demonstrated that a gradient multilayer structure of Weyl semi-metals exhibits robust ATR over a wide range of azimuthal angles.[37] Ma *et al.* recently introduced in-plane anisotropic and magneto-optical materials within the ENZ wavelength range, successfully confining asymmetric thermal radiation to a narrow range of zenith and azimuthal angles (θ:55°–79°, φ: 163.5°–196.5°).[38] Without considering the azimuthal angles, the directional thermal radiation is an azimuthal-integrated nominal one and not enough for practical ATR. To achieve ATR, the design of angularly asymmetric thermal emitters with a specific range of zenith and azimuthal angles is lacking.

Here, we propose a design paradigm for narrow-angle ATR based on a Monte Carlo tree algorithm, which significantly enhances the efficiency of optimal design compared to traditional manual design (TMD) approaches. Utilizing this paradigm, a 24-layer aperiodic multilayer structure composed of magneto-optical materials and dielectric materials is proposed, which can realize ATR within a narrow azimuth range (φ: 165°–195°) at a fixed wavelength ($\lambda = 16\,\mu$m) and a zenith angle ($\theta = 30°$) under TM polarization. Furthermore, we explore the impact of varying zenith angles and the number of layers on the ATR. These findings offer a foundational guide for achieving greater spatial angle control of thermal radiation and enhancing the efficiency of radiation utilization.

II. DESIGN METHODS

Here, a multilayer photonic crystal structure composed of magneto-optical material InAs and dielectric material on top of a perfect reflector is constructed to achieve narrow-angle ATR, as shown in Fig. 1. The incident light is a TM polarized wave and an external magnetic field B is along the y direction. Here, the relative dielectric tensor of InAs is asymmetrical with $B = 3$ T, and the expression is[26]

$$\varepsilon = \begin{bmatrix} \varepsilon_{xx} & 0 & \varepsilon_{xz} \\ 0 & \varepsilon_{yy} & 0 \\ \varepsilon_{zx} & 0 & \varepsilon_{zz} \end{bmatrix}, \tag{1}$$

where

$$\varepsilon_{xx} = \varepsilon_{zz} = \varepsilon_\infty - \frac{\omega_p^2(\omega + i\Gamma)}{\omega[(\omega + i\Gamma)^2 - \omega_c^2]}, \tag{2}$$

$$\varepsilon_{xz} = -\varepsilon_{zx} = i\frac{\omega_p^2\omega_c}{\omega[(\omega + i\Gamma)^2 - \omega_c^2]}, \tag{3}$$

$$\varepsilon_{yy} = \varepsilon_\infty - \frac{\omega_p^2}{\omega(\omega + i\Gamma)}. \tag{4}$$

The specific definitions and parameter values in the above equations are from Ref. 26. In addition, the refractive index of the dielectric material is 1.45. The photonic crystal structure is initially designed with 24 layers (N = 24), resulting in a vast combinatorial space of 2^{24} possible binary sequences. Given the immense scale of this candidate structure space, traditional manual design methods become impractical. To address this challenge and achieve optimized ATR, we employ the Monte Carlo Tree Search (MCTS) algorithm. The detailed optimization process, illustrated in Fig. 1, comprises several key steps: selection, expansion, binary encoding, model construction, simulation, and evaluation. To facilitate the optimization, the two constituent materials are digitized. Specifically, the magneto-optical material InAs is represented by the number 0, while the dielectric material is denoted by the number 1. The algorithm expands from the root node to leaf nodes, generating corresponding binary sequences, such as 010101000001100100100000. Each sequence encodes a unique multilayer structure, and its spectral properties are simulated using the transfer matrix method (TMM).[39] Here, in a reflectance-based nonreciprocal system, the spectral emissivity at a given zenith angle and azimuth ($\epsilon(\lambda, \theta, \varphi)$) is equal to the spectral absorptivity at the opposite zenith angle ($\alpha(\lambda, -\theta, \varphi)$), and the specific expression is[37]

$$\epsilon(\lambda, \theta, \varphi) = \alpha(\lambda, -\theta, \varphi) = 1 - R(\lambda, -\theta, \varphi) - T(\lambda, -\theta, \varphi). \tag{5}$$

In Eq. (5), $R(\lambda, -\theta, \varphi)$ and $T(\lambda, -\theta, \varphi)$ represent spectral reflectance and transmittance at zenith angle $-\theta$ and azimuth angle φ, respectively. In addition, since the bottom of this structure is a perfect reflector, so $T(\lambda, -\theta, \varphi) = 0$. In order to achieve narrow-angle asymmetric thermal radiation, the optimization target *FOM* is

$$FOM = 1/MSE(\text{Opt}, \text{Obj}), \tag{6}$$

where

$$\text{Opt} = \text{abs}(\epsilon(\lambda, \theta, \varphi) - \epsilon(\lambda, -\theta, \varphi)). \tag{7}$$

In Eqs. (6) and (7), *MSE* () represents the mean square error, *Opt* represents the asymmetric degree of the emission spectrum corresponding to each structure, and *Obj* is the target spectrum. In addition, from Eqs. (5) and (7), *Opt* can be converted to the absolute value of the difference between the directional spectral emissivity and the directional spectral absorptivity, i.e., $Opt = abs(\epsilon(\lambda,\theta,\varphi)-\alpha(\lambda,\theta,\varphi))$. In other words, in a nonreciprocal magneto-optical system, the difference between emissivity at opposite zenith angles can be equivalent to the difference between absorptivity and emissivity at the same zenith angle.[26] Here, we consider the ATR within a narrow azimuth at a given wavelength and a zenith angle, and preliminarily set $\lambda = 16\,\mu$m and $\theta = 30°$. The unit layer thickness of InAs (h_{MO}) is about 1.7 μm, and the unit

24 April 2025 09:27:29

© Author(s) 2025

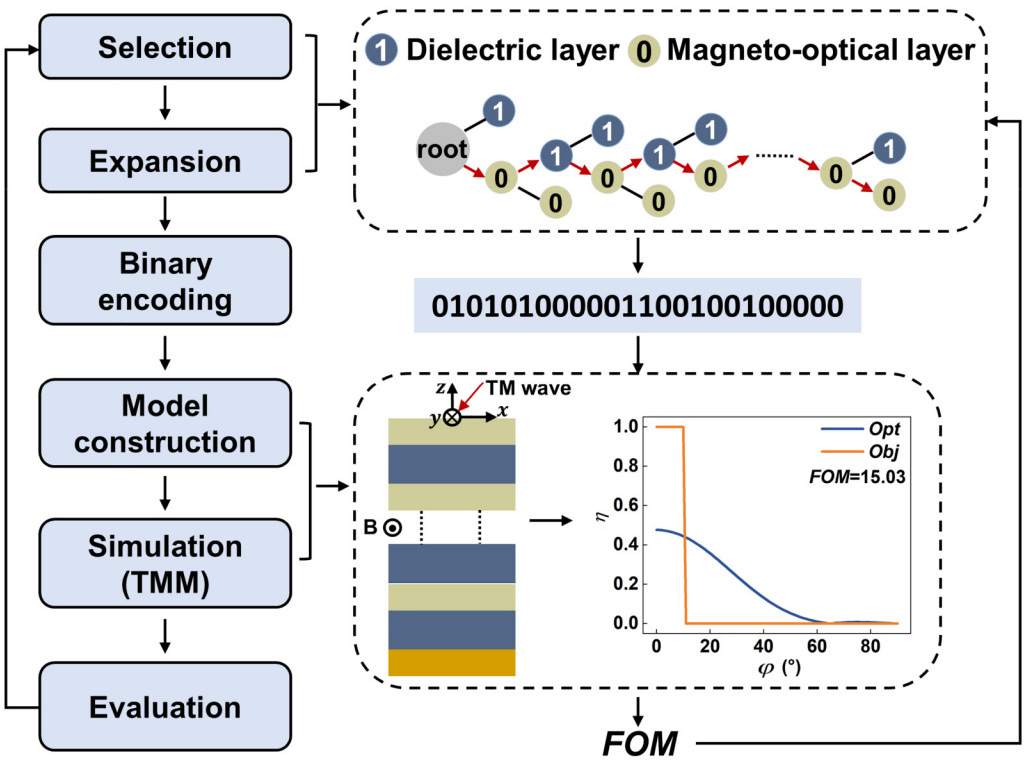

FIG. 1. The roadmap for narrow-angle asymmetric thermal radiation based on a Monte Carlo tree algorithm.

24 April 2025 09:27:29

layer thickness of the dielectric material (h_{die}) is about 2.8 μm. The target spectrum is

$$\text{Obj} = \begin{cases} 1, & 0 \le \varphi \le 10, \\ 0, & 10 < \varphi \le 90. \end{cases} \tag{8}$$

Through the optimization of *FOM*, we can achieve the design of an asymmetric thermal emitter with a small azimuth range, where a higher *FOM* value corresponds to enhanced asymmetry performance. This approach enables efficient exploration of the design space and identification of optimal configurations for achieving the desired thermal emission characteristics.

III. RESULTS AND DISCUSSIONS

Figure 2(a) presents the iterative optimization curve of *FOM*, where the horizontal axis represents the number of iterations and the vertical axis denotes the *FOM* value. It can be seen that *FOM* reaches its maximum (51.3) when the number of iterations is 13 721. Figure 2(b) shows the density distribution of *FOM*, with warmer colors indicating higher concentration. The *FOM* values are predominantly clustered around 10, with only a few instances exceeding 30. Since a higher *FOM* corresponds to better asymmetry, this distribution suggests that achieving strong ATR with a small azimuth range is challenging for most structures. The multilayer structure corresponding to the maximum *FOM* is depicted in Fig. 2(c), with its binary sequence represented as 00101000101010101011001101. Figure 2(d) compares the optimal optimization results with the target spectrum, where the ordinate η represents the degree of asymmetry and the abscissa denotes the azimuth angle. A high degree of asymmetry is maintained for azimuth angles below 10°, gradually decreasing as the azimuth angle increases. To further visualize the emissivity distribution, Fig. 2(e) plots the emissivity as a function of the azimuth angle. The emissivity exhibits an asymmetric distribution centered at $\varphi = 90°$, with strong emission confined to a narrow azimuthal range of 165°–195° and significantly lower emissivity outside this range. This demonstrates the successful realization of ATR within a narrow angular range. To highlight the advantages of this work, a comparative analysis with the previous study[35] is provided in Figs. 2(f) and 2(g). Figure 2(f) shows the asymmetry degree of the other work as a function of azimuth angle, revealing that while high asymmetry is maintained over a wide angular range, achieving narrow-angle asymmetric thermal radiation remains challenging. Figure 2(g) further compares the emissivity distribution of traditional periodic magneto-optical crystal structures under an applied magnetic field. Although these structures exhibit asymmetric thermal radiation, their asymmetry persists over a broad azimuthal range, underscoring the superior performance of the design proposed in this work.

© Author(s) 2025

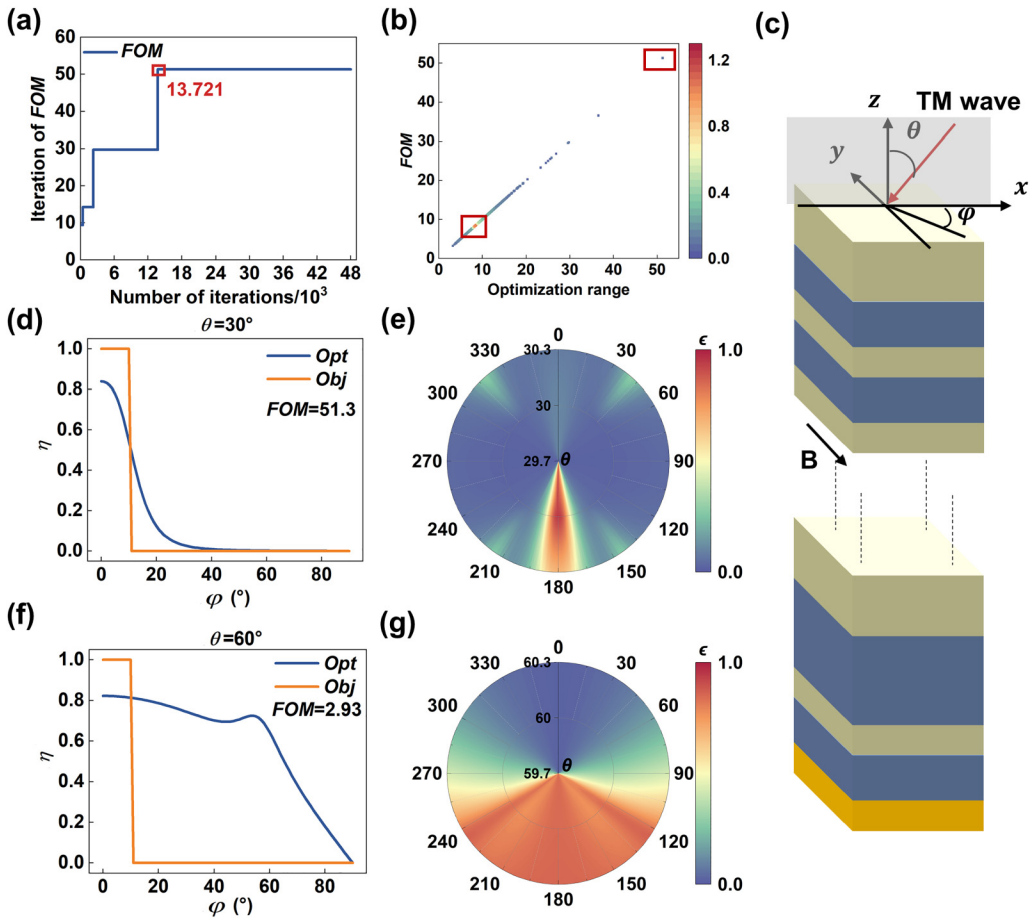

FIG. 2. (a) Tracing of the *FOM* iteration, (b) the density distribution of *FOM* values, (c) the multilayer model corresponding to the optimal result, (d) comparison of the optimal result with the target spectra, (e) the emissivity spectrum corresponding to the optimal result, (f) comparison of another work[35] with the target spectra, and (g) the emissivity spectrum corresponding to another work.[35] Reproduced with permission from Chen *et al.*, Sci. China Technol. Sci. **67**(8) (2024). Copyright 2024 Springer Nature.

To further elucidate the physical mechanism underlying narrow-angle ATR, we analyzed the magnetic field distributions at different azimuthal angles ($\varphi = 0°$ and $\varphi = 60°$) under opposite zenith angles ($\theta = 30°$ and $\theta = -30°$), as illustrated in Fig. 3. First, as depicted in Fig. 3(a), when $\theta = 30°$ and $\varphi = 0°$, the magnetic field distribution in the bottom region of the multilayer structure—specifically, the side in contact with the perfect reflector—exhibits a pronounced standing wave mode. This indicates the occurrence of cavity mode resonance, which facilitates strong absorption. According to Eq. (5), since $\alpha\ (16, 30, 0) = \epsilon\ (16, -30, 0) = \epsilon\ (16, 30, 180)$, strong thermal emission is observed at $\varphi = 180°$, as shown in Fig. 2(e). On the contrary, when $\theta = -30°$ and $\varphi = 0°$, the intensity of the magnetic field distribution inside the multi-layer structure is weaker, which means that the absorption is low, so the emissivity is weak at $\varphi = 0°$. Therefore, the different magnetic field distributions at opposite angles enable the structure to achieve ATR. Additionally, as shown in Figs. 3(c) and 3(d), when $\varphi = 60°$, the magnetic field distributions at opposite zenith angles are nearly identical, indicating the absence of asymmetry. Thus, by calculating the magnetic field distributions at different azimuthal angles, we can effectively explain the origin of narrow-angle asymmetric thermal radiation.

As shown in Fig. 4, further investigation is conducted on the effect of an external magnetic field on ATR. First, the impact of an external magnetic field on the aforementioned optimized best structural sequence (00101000101010101011001101) is explored, as illustrated in Fig. 4(a). When $B = 2$ T, the asymmetry is significantly reduced, and strong asymmetry could no longer be maintained within the desired range of azimuthal angles. This is primarily due to the fact that when the external magnetic field changes, the dielectric tensor of the magneto-optical material also changes accordingly. Consequently, the asymmetric thermal emitter optimized for a 3 T magnetic field is no longer applicable under a 2 T magnetic field. Additionally, when $B = 0$ T, i.e., in the absence of an

24 April 2025 09:27:29

© Author(s) 2025

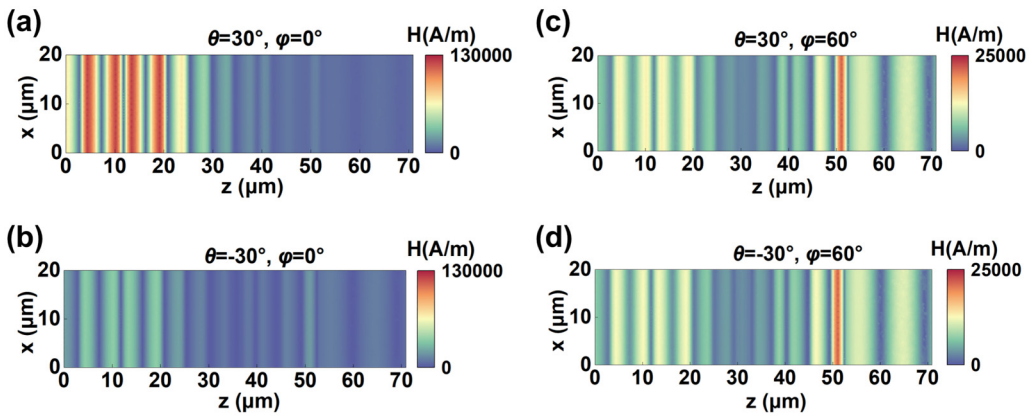

FIG. 3. The magnetic field distribution along the z direction at the wavelength of 16 μm with $B = 3$ T: (a) $\theta = 30°$ and $\varphi = 0°$, (b) $\theta = -30°$ and $\varphi = 0°$, (c) $\theta = 30°$ and $\varphi = 60°$, and (d) $\theta = -30°$ and $\varphi = 60°$.

external magnetic field, no asymmetry existed. This indicates that the asymmetric thermal emitter proposed in this work can only realize ATR under the presence of an external magnetic field, and the structural optimization is performed to further enhance the asymmetry under the influence of the magnetic field. Furthermore, to investigate asymmetry under smaller magnetic fields, when $B = 2$ T, the multi-layer structure is optimized based on the design framework shown in Fig. 1. As shown in Figs. 4(b) and 4(c), when the structural sequence is 001000101010101111110000, strong asymmetric angle thermal radiation could still be achieved within a small range of azimuthal angles.

Figure 5 shows the effect of the number of layers of a multi-layer structure on the narrow-angle ATR. When N = 12, the optimal result is shown in Figs. 5(a) and 5(b), where the maximum *FOM* is 11.2 and the corresponding structural sequence is 101010101110. The asymmetry is obviously weak ($\eta < 0.2$) and cannot be concentrated in a narrow azimuth range. As the number of layers increases to 16 and further to 20, as depicted in Figs. 5(c)–5(f), the asymmetry progressively enhances and becomes more concentrated. This improvement is primarily attributed to the increased number of layers, which facilitates the formation of cavity mode resonances within the structure, thereby amplifying the asymmetry under opposite zenith angles.[40] Therefore, to achieve stronger ATR, we ultimately considered a magneto-optical film with 24 layers, which explains why we selected 24 layers for optimization in the previous discussion.

In addition, the influence of zenith angles on narrow-angle ATR is discussed based on the framework of a Monte Carlo tree algorithm. Here, narrow-angle asymmetric thermal emitters with zenith angles of 20°, 40°, and 60° are optimized, as shown in Fig. 6. When $\theta = 20°$, the maximum value of *FOM* is 17.01, and the corresponding structural sequence is 011111011101110000111010. Compared with Fig. 2(d), the asymmetry is significantly reduced, the maximum asymmetry is about 0.5, and the concentration of asymmetry is significantly weakened. This is mainly because the decrease of the zenith angle weakens the influence of the

24 April 2025 09:27:29

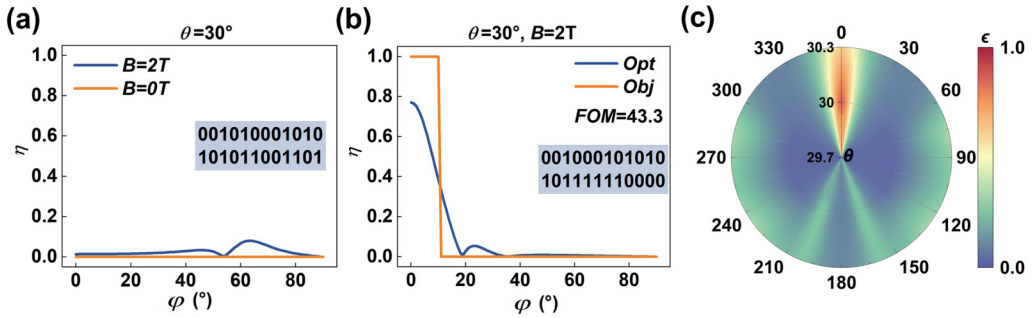

FIG. 4. The influence of the applied magnetic field on ATR. (a) The asymmetry of a multilayer structure corresponding to the sequence (001010001010101011001101) under different magnetic fields with $\theta = 30°$, (b) comparison of the optimized result with the target spectra with $B = 2$ T and $\theta = 30°$, and (c) the emissivity spectrum of the multilayer structure corresponding to the sequence (001000101010101111110000).

© Author(s) 2025

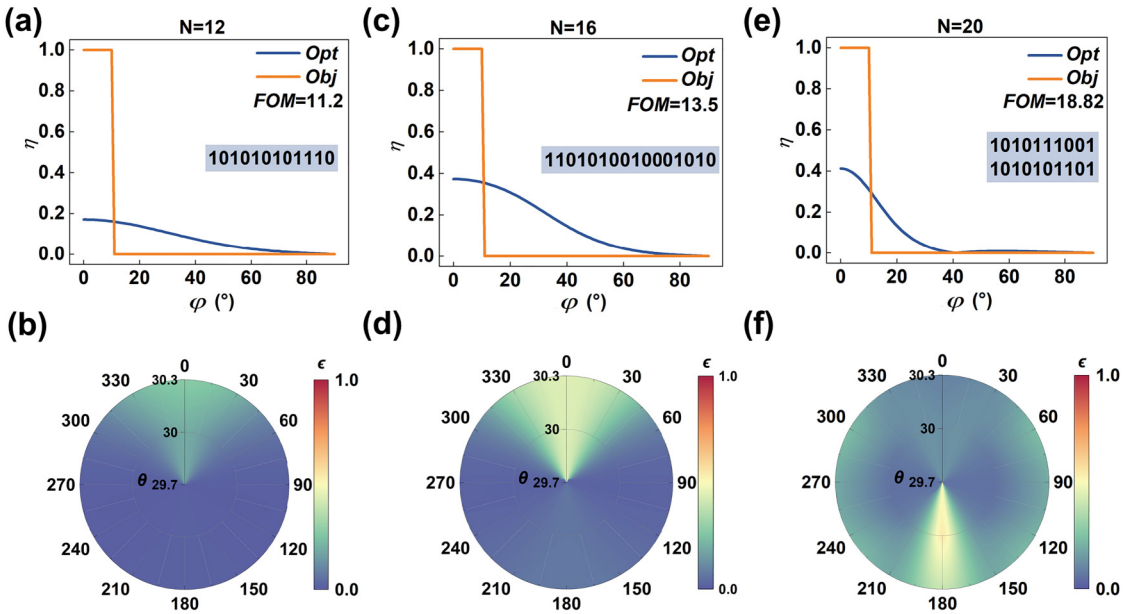

FIG. 5. Optimal results of different layers based on the roadmap: (a) comparison of the optimal result with the target spectra when N = 12, (b) the emissivity spectrum corresponding to the optimal result when N = 12, (c) comparison of the optimal result with the target spectra when N = 16, (d) the emissivity spectrum corresponding to the optimal result when N = 16, (e) comparison of the optimal result with the target spectra when N = 20, and (f) the emissivity spectrum corresponding to the optimal result when N = 20.

24 April 2025 09:27:29

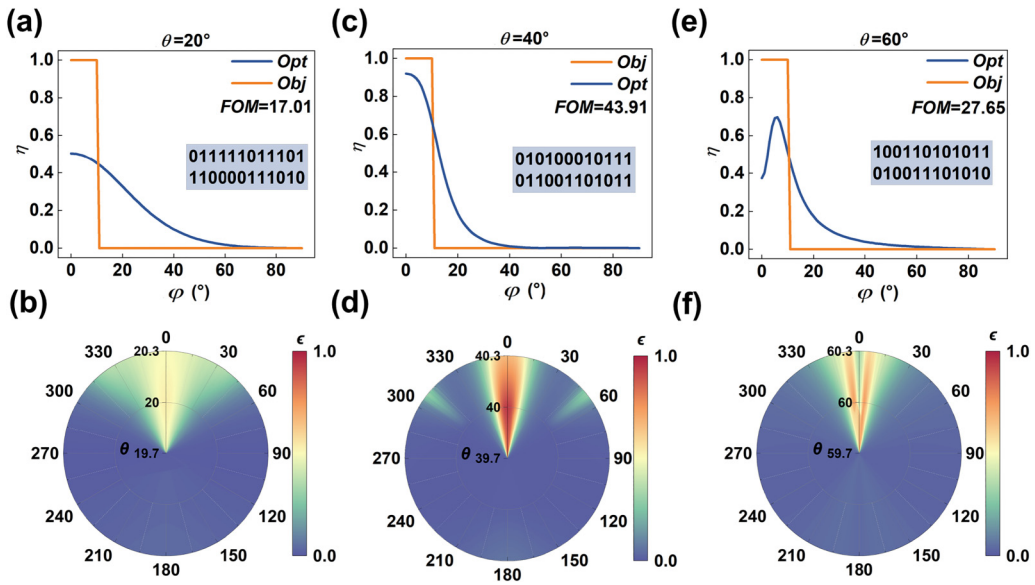

FIG. 6. Optimal results of different zenith angles based on the roadmap when N = 24: (a) comparison of the optimal result with the target spectra when $\theta = 20°$, (b) the emissivity spectrum corresponding to the optimal result when $\theta = 20°$, (c) comparison of the optimal result with the target spectra when $\theta = 40°$, (d) the emissivity spectrum corresponding to the optimal result when $\theta = 40°$, (e) comparison of the optimal result with the target spectra when $\theta = 60°$, and (f) the emissivity spectrum corresponding to the optimal result when $\theta = 60°$.

© Author(s) 2025

asymmetric dielectric tensor of the magneto-optical material, thus reducing the degree of deviation between the emissivity spectra at opposite angles. In addition, as the zenith angle continues to increase to 40°, as shown in Figs. 6(c) and 6(d), the narrow-angle asymmetric thermal radiation presents a certain increase ($\eta = 0.92$). This is mainly because the influence of the asymmetric dielectric tensor on the asymmetry gradually increases with the increase of the zenith angle. However, as the zenith angle increases to 60°, as shown in Figs. 6(e) and 6(f), the asymmetry gradually weakens. This is mainly because the reflection of the multi-layer structure will be significantly enhanced, resulting in certain weakening of the absorption of the structure. As shown in Fig. 6(f), it can be clearly seen that the peak emissivity decreases, resulting in weaker asymmetry.

IV. CONCLUSION

In conclusion, leveraging the Monte Carlo tree algorithm, we have optimized a multi-layer structure to achieve the efficient design of a narrow-angle (φ: 165°–195°) asymmetric thermal emitter under an applied magnetic field. Through comprehensive analysis of the magnetic field distribution at various azimuthal angles, we have identified that the underlying mechanism is predominantly driven by the magneto-optical effect and the excitation of cavity mode resonance, which significantly enhances the narrow-angle asymmetry of thermal radiation. Furthermore, by systematically varying the number of layers from 12 to 24, we observed that reducing the number of layers adversely affects the narrow-angle asymmetry. Additionally, the proposed algorithm framework demonstrates robust performance in designing narrow-angle asymmetric thermal emitter across different zenith angles, highlighting the flexibility and adaptability of this approach. This work not only provides an effective design route for the development of ATR but also holds promise for more efficient energy utilization in applications, such as directional radiation cooling and thermal focusing.

ACKNOWLEDGMENTS

The authors would like to acknowledge the financial support by the National Natural Science Foundation of China (Nos. 92463311, 52422603, 52161160332, and 52411540235), the Natural Science Foundation of Hubei Province (No. 2023AFA072), the Interdisciplinary Research Program of HUST (No. 5003120094), the Fundamental Research Funds for the Central Universities (No. YCJJ20242102) and the open research fund of Suzhou Laboratory (SZLAB-1508-2024-TS016).

AUTHOR DECLARATIONS

Conflict of Interest

The authors have no conflicts to disclose.

Author Contributions

Zihe Chen: Conceptualization (equal); Data curation (equal); Formal analysis (equal); Methodology (equal); Validation (equal); Writing – original draft (equal); Writing – review & editing (equal). **Cheng Yuan:** Formal analysis (equal); Writing – review & editing (equal). **Zhiqiang Wang:** Writing – review & editing (equal). **Wubin Kong:** Writing – review & editing (equal). **Run Hu:** Conceptualization (equal); Formal analysis (equal); Supervision (equal); Writing – original draft (equal); Writing – review & editing (equal).

DATA AVAILABILITY

The data that support the findings of this study are available from the corresponding author upon reasonable request.

REFERENCES

[1]J. Xu, J. Mandal, and A. P. Raman, "Broadband directional control of thermal emission," Science **372**, 393–397 (2021).
[2]Z. J. Coppens and J. G. Valentine, "Spatial and temporal modulation of thermal emission," Adv. Mater. **29**(39), 1701275 (2017).
[3]T. Inoue, M. D. Zoysa, T. Asano, and S. Noda, "Realization of dynamic thermal emission control," Nat. Mater. **13**(10), 928–931 (2014).
[4]R. Hu, J. Song, Y. Liu, W. Xi, Y. Zhao, X. Yu, Q. Cheng, G. Tao, and X. Luo, "Machine learning-optimized Tamm emitter for high-performance thermophotovoltaic system with detailed balance analysis," Nano Energy **72**, 104687 (2020).
[5]S. Zhang, Z. Wu, Z. Liu, and Z. Hu, "An emerging energy technology: Self-uninterrupted electricity power harvesting from the sun and cold space," Adv. Energy Mater. **13**(19), 2300260 (2023).
[6]S. Yu, J.-S. Yu, Z. Chen, Q. Li, Z. Wang, X. Luo, S.-K. Kim, and R. Hu, "Ultrahigh visible-transparency and polymer-free radiative cooling meta-glass coating for building energy saving," ACS Photonics **11**(8), 3412–3423 (2024).
[7]G. T. Park, R. Kang, B. Lee, and S. K. Kim, "Binary-optimization-based multilayers and their practical applications," Curr. Opt. Photonics **8**(6), 545–561 (2024).
[8]K. B. Fan, J. Y. Suen, X. Y. Liu, and W. J. Padilla, "All-dielectric metasurface absorbers for uncooled terahertz imaging," Optica **4**(6), 601–604 (2017).
[9]J. Y. Ma, Y. Ma, and C. Li, "Infrared and visible image fusion methods and applications: A survey," Inf. Fusion **45**, 153–178 (2019).
[10]M. S. Long, Y. Wang, P. Wang, X. H. Zhou, H. Xia, C. Luo, S. Y. Huang, G. W. Zhang, H. G. Yan, Z. Y. Fan, X. Wu, X. S. Chen, W. Lu, and W. D. Hu, "Palladium diselenide long-wavelength infrared photodetector with high sensitivity and stability," ACS Nano **13**(2), 2511–2519 (2019).
[11]Z. G. Pan, Y. Zhang, Z. Z. Cheng, J. M. Tong, Q. Y. Chen, J. P. Zhang, J. X. Zhang, X. Li, and Y. J. Li, "Sensing properties of a novel temperature sensor based on field assisted thermal emission," Sensors **17**(3), 473 (2017).
[12]Y. K. Chen, B. X. Wang, and C. Y. Zhao, "Dual-band spatially-distinguishable metasurface thermal emitter for filterless mid-infrared gas sensing," Int. J. Therm. Sci. **185**, 108069 (2023).
[13]Z. G. Pan, Y. Zhang, and C. H. Zhang, "Modelling of carbon nanotube film based temperature sensor: Thermal emission and gas discharge," Nanotechnology **32**(47), 475502 (2021).
[14]D. Costantini, A. Lefebvre, A. L. Coutrot, I. Moldovan-Doyen, J. P. Hugonin, S. Boutami, F. Marquier, H. Benisty, and J. J. Greffet, "Plasmonic metasurface for directional and frequency-selective thermal emission," Phys. Rev. Appl. **4**(1), 014023 (2015).
[15]J. Yu, R. Qin, Y. Ying, M. Qiu, and Q. Li, "Asymmetric directional control of thermal emission," Adv. Mater. **35**(45), e2302478 (2023).
[16]J.-J. Greffet, R. Carminati, K. Joulain, J.-P. Mulet, S. Mainguy, and Y. Chen, "Coherent emission of light by thermal sources," Nature **416**, 61–64 (2002).
[17]J.-W. Cho, Y.-J. Lee, J.-H. Kim, R. Hu, E. Lee, and S.-K. Kim, "Directional radiative cooling via exceptional epsilon-based microcavities," ACS Nano **17**(11), 10442–10451 (2023).
[18]M. M. Hossain, B. Jia, and M. Gu, "A metamaterial emitter for highly efficient radiative cooling," Adv. Opt. Mater. **3**(8), 1047–1051 (2015).
[19]W. Li, Y. Shi, Z. Chen, and S. Fan, "Photonic thermal management of coloured objects," Nat. Commun. **9**(1), 4240 (2018).

24 April 2025 09:27:29

© Author(s) 2025

[20]M. Lee, G. Kim, Y. Jung, K. R. Pyun, J. Lee, B. W. Kim, and S. H. Ko, "Photonic structures in radiative cooling," Light: Sci. Appl. **12**(1), 134 (2023).
[21]J. E. Moore and L. Balents, "Topological invariants of time-reversal-invariant band structures," Phys. Rev. B **75**(12), 121306 (2007).
[22]A. C. Overvig, S. A. Mann, and A. Alù, "Thermal metasurfaces: Complete emission control by combining local and nonlocal light-matter interactions," Phys. Rev. X **11**(2), 021050 (2021).
[23]K. Ito, T. Matsui, and H. Iizuka, "Thermal emission control by evanescent wave coupling between guided mode of resonant grating and surface phonon polariton on silicon carbide plate," Appl. Phys. Lett. **104**(5), 051127 (2014).
[24]J. Zhou, T. G. Chen, Y. Tsurimaki, A. Hajj-Ahmad, L. Fan, Y. Peng, R. Xu, Y. Wu, S. Assawaworrarit, S. Fan, M. R. Cutkosky, and Y. Cui, "Angle-selective thermal emitter for directional radiative cooling and heating," Joule **7**(12), 2830–2844 (2023).
[25]F. Xie, W. Jin, J. R. Nolen, H. Pan, N. Yi, Y. An, Z. Zhang, X. Kong, F. Zhu, K. Jiang, S. Tian, T. Liu, X. Sun, L. Li, D. Li, Y.-F. Xiao, A. Alu, S. Fan, and W. Li, "Subambient daytime radiative cooling of vertical surfaces," Science **386**(6723), 788–794 (2024).
[26]L. Zhu and S. Fan, "Near-complete violation of detailed balance in thermal radiation," Phys. Rev. B **90**(22), 220301 (2014).
[27]B. Zhao, Y. Shi, J. Wang, Z. Zhao, N. Zhao, and S. Fan, "Near-complete violation of Kirchhoff's law of thermal radiation with a 0.3 T magnetic field," Opt. Lett. **44**(17), 4203–4206 (2019).
[28]Z. Chen, S. Yu, C. Yuan, X. Luo, and R. Hu, "Near-normal nonreciprocal thermal radiation with a 0.3 T magnetic field based on double-layer grating structure," Int. J. Heat Mass Transf. **222**, 125202 (2024).
[29]K. J. Shayegan, S. Biswas, B. Zhao, S. Fan, and H. A. Atwater, "Direct observation of the violation of Kirchhoff's law of thermal radiation," Nat. Photonics **17**, 891–896 (2023).
[30]K. J. Shayegan, B. Zhao, Y. Kim, S. Fan, and H. A. Atwater, "Nonreciprocal infrared absorption via resonant magneto-optical coupling to InAs," Sci. Adv. **8**, eabm4308 (2022).
[31]Z. Chen, S. Yu, and R. Hu, "Bridging the Fabry–Perot cavity and asymmetric Berreman mode for long-wave infrared nonreciprocal thermal emitters," Sci. China Technol. Sci. **67**(10), 3285–3293 (2024).
[32]Z. Zhang and L. Zhu, "Broadband nonreciprocal thermal emission," Phys. Rev. Appl. **19**(1), 014013 (2023).
[33]M. Liu, S. Xia, W. Wan, J. Qin, H. Li, C. Zhao, L. Bi, and C.-W. Qiu, "Broadband mid-infrared non-reciprocal absorption using magnetized gradient epsilon-near-zero thin films," Nat. Mater. **22**, 1196–1202 (2023).
[34]M. Luo, Y. Xu, Y. Xiao, and G. Yu, "Strong nonreciprocal thermal radiation by optical Tamm states in Weyl semimetallic photonic multilayers," Int. J. Therm. Sci. **183**, 107851 (2023).
[35]Z. Chen, S. Yu, C. Yuan, X. Cui, and R. Hu, "Defect-mode and Fabry–Perot resonance induced multi-band nonreciprocal thermal radiation," Sci. China Technol. Sci. **67**(8), 2405–2412 (2024).
[36]J. Wu, Z. Wang, B. Wu, Z. Shi, and X. Wu, "The giant enhancement of nonreciprocal radiation in Thue-Morse aperiodic structures," Opt. Laser Technol. **152**, 108138 (2022).
[37]K. Shi, Y. Sun, R. Hu, and S. He, "Ultra-broadband and wide-angle nonreciprocal thermal emitter based on Weyl semimetal metamaterials," Nanophotonics **13**(5), 737–747 (2024).
[38]Y. Ma, J. Wang, L. Li, T. Liu, and W. Li, "Broadband unidirectional thermal emission," Laser Photonics Rev. **19**(2), 2400716 (2025).
[39]L. Wang, F. J. García de Abajo, and G. T. Papadakis, "Maximal violation of Kirchhoff's law in planar heterostructures," Phys. Rev. Res. **5**(2), L022051 (2023).
[40]J. Wu and Y. M. Qing, "Strong nonreciprocal radiation with topological photonic crystal heterostructure," Appl. Phys. Lett. **121**(11), 112201 (2022).

24 April 2025 09:27:29

© Author(s) 2025